physica status solidi pss a
www.pss-a.com

Development and Fabrication of Microdosimeter Arrays Based on Single-Crystal Diamond Schottky Diodes

*Claudio Verona, Gianluca Verona Rinati, Giuseppe Schettino, and Gabriele Parisi**

The interest in microdosimetry is growing thanks to the advancement in microdosimetric technologies, improving detector performance and reliability. Herein, the fabrication and characterization of a novel diamond-based microdosimeter are proposed. The microdosimeter consists of an array of single-crystal diamond Schottky diodes about 1.5 μm thick connected in parallel. The detector prototypes are characterized using the ion beam-induced charge technique, employing a 6 MeV carbon ions microbeam. Despite a good overall response, the first prototypes are affected by the "bridge effect": a charge collection beneath the metallic bridges connecting the sensitive volumes (SVs), which alters the energy deposition spectrum. To mitigate the bridge effect, different technological solutions are explored: the selective growth of intrinsic diamond layers and the use of an insulating material such as photoresist. These second prototypes reveal a good SV spatial definition without any charge collection from the bridges and a good response homogeneity within the SVs ranging between 3% and 5% full-width-half-maximum among the different prototypes. While the cell-like thickness and lateral dimensions of SVs make the diamond microdosimeter array ideal for radiobiological applications, its array configuration can make it highly versatile to perform under different fluence rate conditions in particle therapy.

1. Introduction

Microdosimetry measures the stochastic energy distributions deposited by the radiation in a micrometric sensitive target volume comparable to the size of a human cell. This technique can be used, for instance, to estimate the relative biological effectiveness (RBE) of hadron therapy beams.[1,2] With the aim of mimicking biological sites to better describe the physics behind the biological effects of radiation, different microdosimetric technologies have been developed.[3,4] The ideal microdosimeter should have a cross-sectional size, a shape, and an atomic composition comparable to human cells. The sensitive volume (SV) of the microdosimeter should therefore meet three main requirements: 1) having both its lateral and longitudinal sizes of the order of a few μm; 2) being made of tissue-equivalent material; and 3) being well defined with a homogeneous charge collection, and no charge should be collected from outside.

Tissue equivalent proportional counters (TEPCs) are traditionally considered the reference microdosimeters.[5–7] The TEPC is based on low-pressure gas (propane) to simulate a micron-sized SV confined into a solid wall made of tissue-equivalent plastic. Microdosimetric measurements with TEPCs were successfully used to assess the RBE of different radiation beams.[8–11] However, the TEPC has several limitations including the wall effects, high voltage operation, and a large physical size (mm scale) which limits both the spatial resolution and the particle fluence rate capability of the detector.

Solid-state microdosimeters were developed[12] as an alternative to the TEPC, as they do not require gas, can be operated at low voltages, are cheaper, and have a better portability than TEPCs. Their microscopic physical size gives a good spatial resolution and allows to use them in high-intensity beams. In addition, they can be fabricated in an array configuration to mimic biological cells arrays. Such configuration would also optimize the detection performances of the microdosimeter. Indeed, the array geometry is characterized by low capacitance improving the noise threshold and by a SV size comparable to a cell improving the accuracy of the delta rays contribution measured.[13] The possibility to connect and read each single SV individually or in groups would allow for measurement time optimization. At low fluence rate, like those found in the distal part of the Bragg curve or in the out-of-field regions of a therapeutic particle beam, the large overall sensitive area helps to reduce measurement time. At high fluence rate, like those found in the entrance region of a clinical beam, the individual SV

C. Verona, G. Verona Rinati
Dipartimento di Ingegneria Industriale
Università di Roma "Tor Vergata"
Sez. INFN-Roma2, Rome 00133, Italy

G. Schettino, G. Parisi
Medical Radiation Science Group
National Physical Laboratory – NPL
Teddington TW11 0LW, UK
E-mail: gabriele.parisi@unipv.it

G. Parisi
Department of Physics
University of Surrey
Guildford GU2 7XH, UK

The ORCID identification number(s) for the author(s) of this article can be found under https://doi.org/10.1002/pssa.202300987.

DOI: 10.1002/pssa.202300987

reading (or the reading of smaller groups of SVs) would avoid pile-up issues while still exploiting a large overall sensitive area. In addition, the array microdosimeter (AμDOS) is made of individual SVs with high spatial resolution that can be used for a pixelated characterization of critical areas, e.g., organs-at-risk and penumbras, as well as out-of-field regions.

Silicon microdosimeters in array configuration were developed at Politecnico di Milano,[14] at University of Wollongong[15,16] and at the Spanish National Center of Microelectronics.[17,18] These have been employed for the characterization of clinical particle beams, showing a good agreement with the results from the well-established TEPC. Nevertheless, they do possess certain constraints, such as lacking water equivalence, the complexity of the microtechnology manufacturing processes involved, and the potential degradation of performance due to radiation damage over time.

The interest in synthetic diamond is attributed to its outstanding properties such as high radiation tolerance and near-tissue equivalence for a wide range of radiation qualities used in radiation therapy.[19,20] Diamond-based microdosimeters have been proposed by the University of Wollongong in Australia,[21,22] by the Diamond Sensors Laboratory of CEA in France,[23,24] and by the University of Roma "Tor Vergata" in Italy.[25,26]

The diamond microdosimeter prototype presented in ref. [21] was fabricated using the focused ion beam techniques. It featured 3D vertical walls with SVs embedded in a diamond matrix. The 3D SVs were not fully isolated but were defined by the lateral electric field induced by two electrodes. The prototypes showed a nonuniform charge collection efficiency (CCE) within the SVs. Patterned laser ablation was later employed to create an array of 3D diamond cylindrical SV structures, as reported in ref. [22]. The microfabrication method, however, was excessively complex, and it should be noted that the authors have not succeeded in fabricating a functional device based on this geometry yet. The diamond microdosimeter described in ref. [23] was realized in an array configuration based on two different junction regions: a p+–intrinsic diamond–metal junction defining the SVs and a metal–intrinsic diamond–metal junction outside. This technology could only operate in an unbiased mode, i.e., 0 V. Signals were otherwise generated in the area surrounding the SVs, resulting in a single macro-SV. However, at zero bias voltage, the CCE of the prototype resulted incomplete for heavy ions such as carbon ions. A second microdosimeter prototype based on metal–intrinsic diamond–metal configuration is described in ref. [24] featuring an array of SVs encircled by a guard ring electrode. Each SV had a diameter of 60 μm and was connected to adjacent SVs by 10 μm thin connecting bridges which were electrically active, similar to the SVs.

Considering the state of the art highlighted here, this work aims to develop a diamond AμDOS with well-defined SVs designed specifically to ensure the accuracy of radiation quality measurements for particle beam delivery. Novel designs are proposed to find a solution to the main challenges affecting the SV definition and the detector performances, such as the signal collection from the bridges connecting the SVs.

In this work, the development, fabrication, and characterization of a novel diamond-based microdosimeter arranged in array configuration are reported. The microdosimeter consists of an array of circular Schottky diodes based on boron-doped/intrinsic diamond/metal configuration connected in parallel to a single-channel readout electronics. Each SV has a diameter that varies from 10 to 50 μm between different prototypes. The adopted geometry could allow reading each SV separately. The cylindrical shape of the SV is intended to replicate the form of a biological cell and offers a more isotropic volume compared to a cubic design. In addition, the boron-doped/intrinsic diamond/Schottky metal configuration showed good spectroscopic performances as well as high radiation hardness.[25,26] The maps of CCE of the developed microdosimeters were investigated by means of the ion beam-induced charge collection (IBIC) technique in two experiments: at the ion beam facility of Ruđer Boskovic Institute in Zagreb (Croatia) and at the Surrey Ion Beam Centre in Guildford (UK).

2. Experimental Section

2.1. The Diamond AμDOSs

The diamond AμDOS was fabricated and developed at the Industrial Engineering Department of Tor Vergata University of Rome laboratories. The device consists of an array of Schottky diodes fabricated on the same low-cost diamond substrate. The diodes were realized combining both microwave-enhanced chemical vapor deposition (CVD) of synthetic single crystal diamond and photolithography techniques. The fabrication process, schematically reported in **Figure 1**, can be outlined as follows: a) A chromium layer, about 200 nm in thickness, was first thermally evaporated on a cleaned commercial low-cost diamond substrate and patterned using a positive photoresist, as schematically shown in Figure 1a. This Cr layer acts as a plasma-resistant mask that allows the selective growth of synthetic diamond on the regions where the diamond substrate was left naked by the patterned Cr layer. It is worth noting that the selection of the Cr layer over other metals is attributed to its adhesion to the diamond surface and resistance to diamond deposition temperatures, i.e., 600 °C. b) A boron heavily doped diamond layer of about 0.3 μm thickness was selectively grown by CVD on diamond substrate surface. Two slightly different geometries were developed for the prototypes, with cylindrical SVs with diameters of 10 and 40 μm. The SVs were connected by horizontal tracks with widths of about 4 and 8 μm, respectively (Figure 1b). Such a conductive layer is used as the back contact of the microdosimeter. The resistivity of boron-doped layer was estimated about 1 kΩ sq^{-1}. c–d) The chromium film was removed by wet etching, and a square shaped intrinsic diamond film was selectively grown to about 1.6 ± 0.1 μm in thickness by using a second Cr plasma-resistant mask realized by photolithography technique (see Figure 1c,d). Such an intrinsic diamond layer is used as the sensitive layer of the microdosimeter. e) The chromium was etched, and the sample was carefully cleaned and oxidized by isothermal annealing in air at 500 °C to remove the hydrogenated surface conductive layer (see Figure 1e). f) An 80 nm thick chromium layer, working as upper electrode, was evaporated and carefully patterned as the boron-doped diamond back-contact by photolithographic technique. The superficial electrodes obtained were aligned on the doped ones (see Figure 1f). The electrodes were connected to a common bond

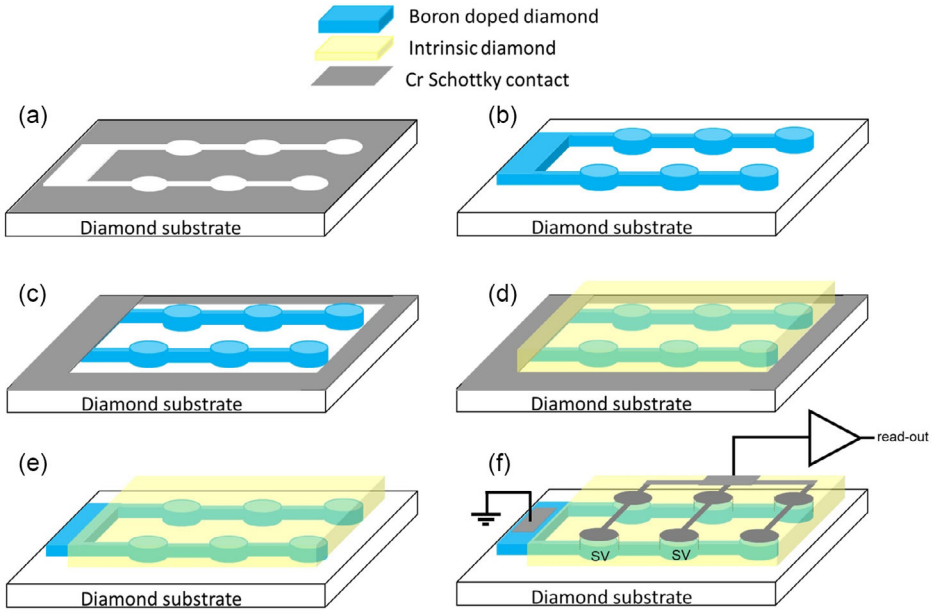

Figure 1. a–f) Schematic diagram of the fabrication process of the AμDOS device.

pad, thus providing a single readout channel. It is worth noting that the proposed structure would allow for connecting the electrodes separately as well.

Figure 2 shows light microscope (LM) images and atomic force microscope (AFM) pictures of the developed AμDOSs. With this design, a square array of circular-shaped diamond micro-SVs behaving like Schottky diodes in a boron-doped/intrinsic diamond/Cr configuration was obtained.

As it can be observed clearly in Figure 2, the array consists of 1.6 μm thick micro-SVs interconnected by thin connecting bridges. The microdosimeter with 40 μm diameter (large) diodes has 5×5 SVs with 40 μm pitch covering an area of 360×360 μm^2.

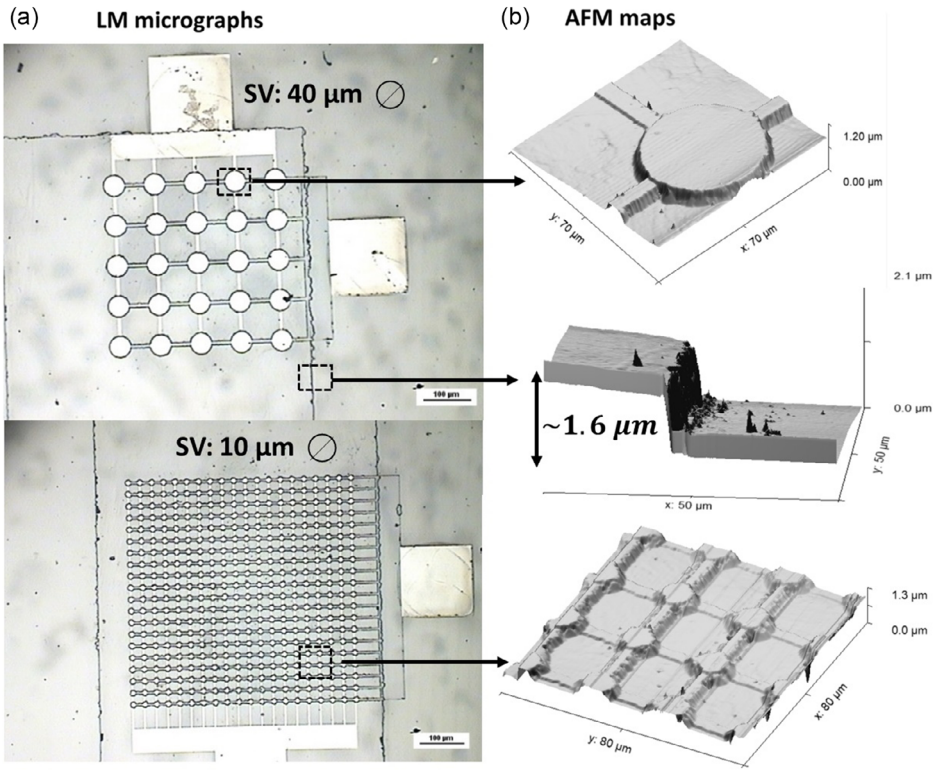

Figure 2. a) LM micrographs of the two AμDOSs (left side) and b) AFM maps of the SVs of the AμDOSs (right side).

The microdosimeter with 10 μm diameter (small) diodes has 20 × 20 SVs with 15 μm pitch covering a 485 × 485 μm^2 area.

2.2. Further Development of the Diamond AμDOS

After characterizing the performances of the first prototypes manufactured, two different technological solutions were developed to prevent charge collection from the bridges connecting the SVs. Both solutions are based on the manufacturing process previously described.

The first approach consists of including the selective growth of the intrinsic diamond layer on top of the boron-doped one. The fabrication process is the same as reported before, with the exception that the intrinsic layer is grown in a cylindrical shape only in the zones where the actual SVs will be created. The second approach, instead, consists of spin coating a positive resist film with a thickness of about 3 μm onto diamond surface after the step (e) depicted in Figure 1. By exposing only the circular areas above the SVs to UV light, direct access to the intrinsic CVD diamond layer is created only in correspondence with the SVs. To enhance its thermal and chemical stability, the positive resist was hard-baked at 180 °C on a hot plate. A chromium electrode is then thermally evaporated on both photoresist and intrinsic diamond surface. In this way, the Schottky diodes in a boron-doped/intrinsic diamond/Cr configuration are surrounded by the positive photoresist, and thus completely isolated. A prototype was manufactured for each of the two approaches: the AμDOS-SG according to the selective growth of the intrinsic layer approach and the AμDOS-IL according to the patterned isolation layer deposition approach. The two devices had SVs of 50 μm diameter and, respectively, 1 ± 0.1 and 1.5 ± 0.1 μm in thickness. The two prototypes are schematized in **Figure 3**.

2.3. IBIC Characterizations

The IBIC characterization was performed to study the detectors response in terms of their charge collection properties and uniformity. IBIC measurements exploit a focused beam which is scanned on the detector surface and which position is known. This allows for a detailed mapping of the CCE across the detector surface. The measurement spatial resolution is dictated by the microbeam spot size, which was estimated to be ≈1 μm in both the microbeam facilities the experiments were carried out. An ion microprobe facility is usually equipped with a magnetic quadrupole lens and a magnetic scanner unit capable of focusing the beam to micrometric sizes and raster scanning it on the detector surface.

The developed devices were characterized in two different facilities: the ion microbeam facility of the Ruđer Boskovic Institute (RBI) in Zagreb (Croatia)[27] and the Surrey Ion Beam Centre in Guildford (UK).[28,29] In both cases, the radiation quality was a 6 MeV carbon ion beam from a tandem Van der Graaff accelerator. The penetration depth of 6 MeV carbon ions in diamond is about 2.79 μm, in accordance with SRIM Monte Carlo simulation.[30] Consequently, only a portion of the impinging carbon energy is transferred to the sensitive layer of the diamond prototypes. The detectors were fixed on a dedicated sample holder and placed inside the vacuum chamber of the microbeam line. The ion current was carefully reduced to obtain a detection count rate of about 1 kcps, ensuring optimal interaction with the diamond detector without saturating the charge collection. The amount of energy deposited in the diamond microdosimeter was measured using a charge sensitive preamplifier (Ortec 142) and a shaping amplifier (ORTEC 570) with 3 μs shaping time to optimize pileup and reduce noise. The signal was fed directly to a dedicated analog-to-digital converter connected to the computer for data acquisition. For each event triggered, the charge collected, as well as the beam position coordinates *xy*, was stored into an event-by-event list mode file. The collected charge and corresponding beam position coordinates were meticulously analyzed and processed to create IBIC median charge collection maps, revealing spatial correlations in energy distribution over the scanned area. The energy calibration was performed using a pulse generator and a thick silicon detector with 100% CCE in response to the same ion species.

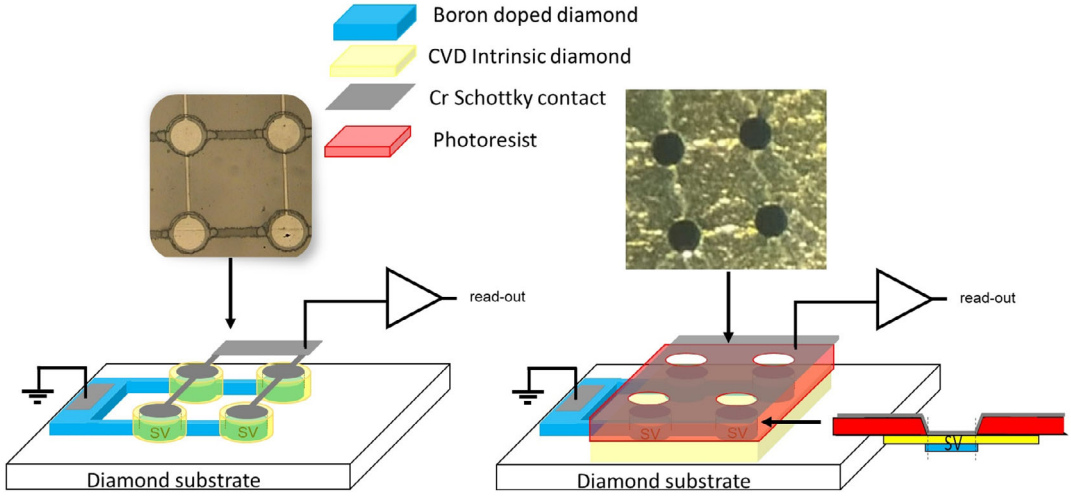

Figure 3. Schematic representation of the AμDOS-SG (left side) and AμDOS-IL (right side) prototypes.

3. Results and Discussion

The characterization of the AμDOS by means of 6 MeV C ions microbeam scanning at different locations is presented, with an analysis of the main inhomogeneities found in the detector response. **Figure 4** shows a large IBIC map (≈ 500 × 500 μm^2) of the AμDOS first version with SVs' diameter of 10 μm. The map was oriented as in the optical microscope picture of Figure 2. As can be noticed, the most external SVs suffered from lower CCE. These SVs are laterally and longitudinally the furthest from the metallic and the boron-doped diamond common pads connected to the electronics. Being the furthest from where the voltage was applied, the resistance encountered along the electrodes path lowered the effective bias that gets to the SV there. This inhomogeneity could be overcome by reducing the resistivity of the boron-doped diamond layer and by applying an even higher bias voltage.

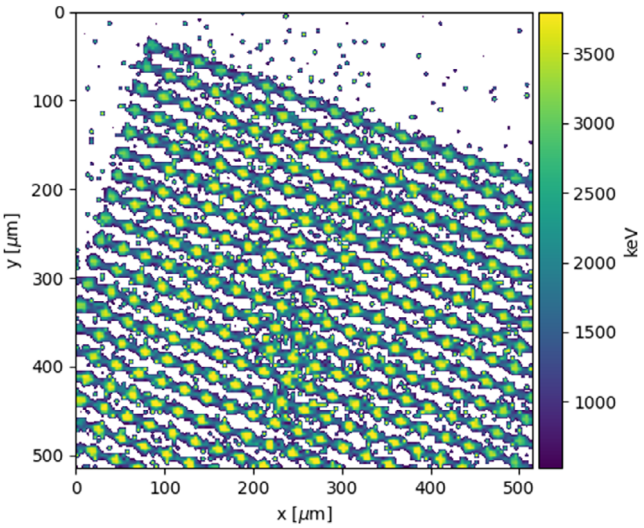

Figure 4. Large IBIC map of the 10 μm diameter AμDOS prototype. The measurement was collected at the RBI (Zagreb, Croatia) using a 6 MeV carbon ions microbeam.

Additionally, a small blurred region is visible on the map due to defects and issues in the lithography process, resulting in imperfect pattern transfer. Finally, an incomplete charge collection could be observed around the SVs and beneath the metallic bridges. This region compromised both the energy deposition spectrum and the SV spatial definition, as the bridges are not meant to be collecting any signal. The effect of such region of incomplete charge collection will be studied in detail later in this section.

Figure 5 shows the IBIC map and profile of one of the 40 μm diameter SVs, as well the energy deposition spectrum collected inside the SV. The spectrum inside the SV showed the typical Gaussian distribution of energy deposition expected for a monoenergetic beam crossing the detectors. The response homogeneity within the SVs was estimated by fitting the spectrum with a Gaussian function and by considering the resulting full-width-half-maximum (FWHM). A good homogeneity around 5% FWHM was found for both prototypes. The energy spectrum was also compared with a Monte Carlo simulation carried out by means of SRIM.[30] The comparison, which is shown in

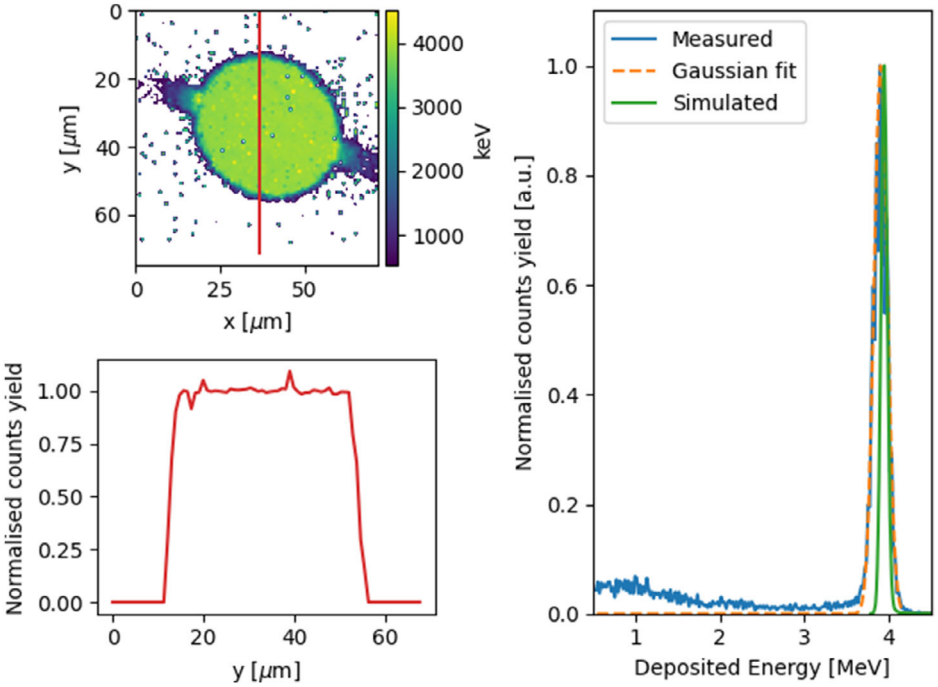

Figure 5. (Top-left) IBIC map of one of the SVs of the 40 μm diameter AμDOS prototype. (Bottom-left) CCE profile of the same SV at $x = 36.5$ μm; a red line visually locates the profile on the IBIC map. (Right) The deposited energy spectrum measured by the 40 μm diameter AμDOS prototype when irradiated by a 6 MeV carbon ions microbeam at the RBI (Zagreb, Croatia); the Gaussian fit through which the response homogeneity was estimated, and a simulation carried out by means of SRIM is also represented.

Figure 5 for the 40 μm diameter AμDOS prototype, allowed to estimate the CCE of the detector. It is worth stressing that such CCE value is not a direct measurement of the detector CCE but, relying on Monte Carlo simulations, it is an estimate. Its error margin reflects the uncertainty of the stopping power values used by SRIM code. As suggested in ref. [30], SRIM stopping power uncertainty can be considered about 5%. The position of the energy deposition peak was observed to differ of 1%, allowing to estimate a CCE of ≈99% and surely higher than 94% considering the error margin due to stopping power uncertainty. Further, a good spatial definition of the SVs was obtained for both the detectors with no charge collection outside the SVs' area. Analyzing the CCE profiles, they were estimated to drop from 90% to 10% within 2.5 μm.

However, the bridge effect had a significant impact on the detector response. Hence, a detailed analysis of its criticality was carried out. The effect was isolated by scanning the microbeam on a subregion of the array's sensitive area, including only a few SVs. The results of the IBIC analysis for the 10 and 40 μm diameter SVs are shown in **Figure 6** and **7**, respectively.

As can be observed in the energy deposition spectra in Figure 6 and 7, the Gaussian-shaped energy distribution was perturbed by a low-energy tail. The spectra were therefore divided into energy regions to investigate the origin of the low energy tail in more detail. A partial IBIC map was then created for each region by considering only those events falling within the region's energy window. The regions were defined in order to isolate the low energy tail from the main energy deposition peak and to try to spot any particular behavior that could have been associated with the bridges. Hence, a first region (the red region, referring to Figure 6 and 7) was chosen to isolate the main energy deposition peak. As a peak-like structure was observed in the low energy tail, a second region (the orange region) was defined by trying to isolate such structure. This feature was particularly evident in Figure 6. Two additional regions were eventually defined: the green region between the main peak and the second peak-like structure, and the blue region to cover the lower energy part of the tail. Such division of the spectra in four energy regions allowed to effectively interpret the results: 1) The events contributing to the main peak were collected by very well-defined SVs, showing homogeneous response as reported in Figure 5. 2) The higher energy side of the low-energy tail (green region) only had the contribution from those events collected with incomplete charge collection at the SVs' borders. 3) The peak-like structure (orange region) was created instead by the combination of events detected at the SVs' border and of events detected by the bridges connecting the SVs. 4) The lower energy side of the low-energy tail (blue region) is generated by the charge collected from a more external part of both SVs' borders and bridges.

The low-energy tail perturbation was therefore the result of two similar but separate effects: the border effect and the bridge effect. The border effect is due to the charge diffusion from regions surrounding the SV, and it has long been known to affect solid-state microdosimeters.[16,20,26,31] While the border effect is a more general problem of solid-state microdosimeters, the bridge effect specifically affects AμDOSs. Besides the AμDOS, indeed, the bridge effect had already been reported affecting the first generations of silicon AμDOS.[32,33] Hence, this work will focus on the analysis of the bridge effect and its resolution. A dedicated study to investigate the border effect in diamond

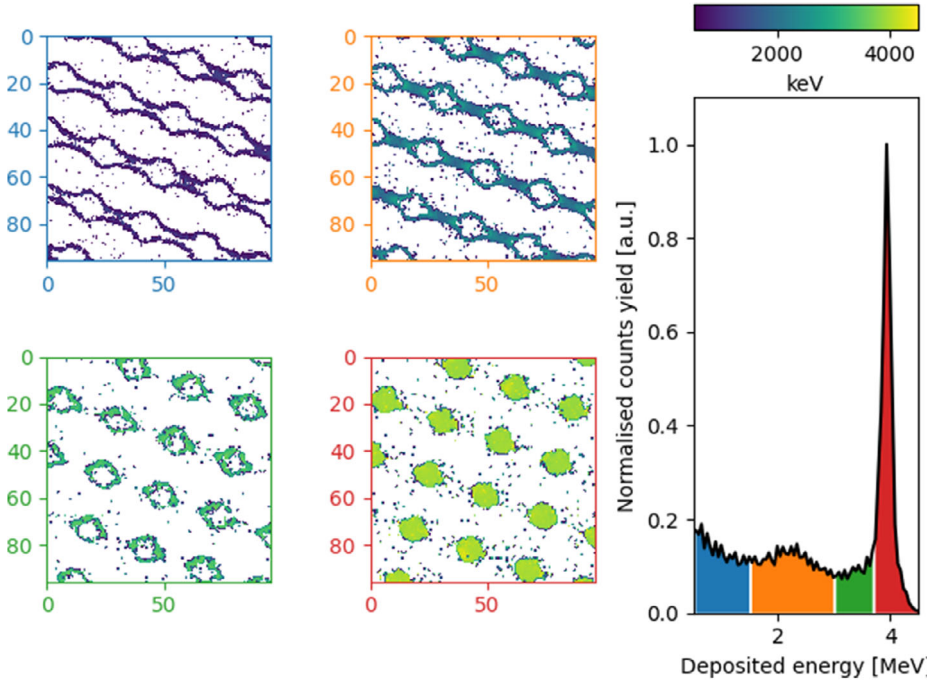

Figure 6. (Right) Deposited energy spectrum measured by the 10 μm diameter AμDOS prototype when irradiated by a 6 MeV carbon ions microbeam at the RBI (Zagreb, Croatia); the spectrum is divided in four regions, each one represented by a different color. (Left) The IBIC maps corresponding to each region, created by considering only events whose energy deposition occurred within the region considered; the color of the maps contour is the same color as the corresponding region.

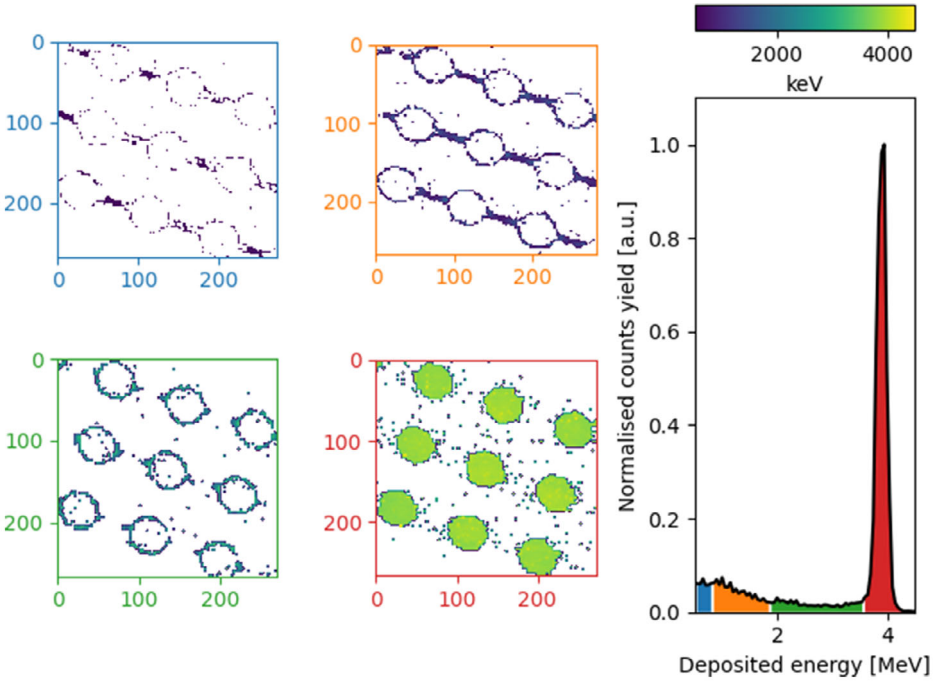

Figure 7. (Right) Deposited energy spectrum measured by the 40 μm diameter AμDOS prototype when irradiated by a 6 MeV carbon ions microbeam at the RBI (Zagreb, Croatia); the spectrum is divided in four regions, each one represented by a different color. (Left) The IBIC maps corresponding to each region, created by considering only events whose energy deposition occurred within the region considered; the color of the maps contour is the same color as the corresponding region.

microdosimeters and its impact to microdosimetry is foreseen in the near future by the authors.

The shared contribution from bridges and borders to the mean deposited energy measured, c_ε, could be estimated according to the following equation:

$$c_\varepsilon = \frac{\sum_i^N \int_{S_i} \varepsilon f(\varepsilon) d\varepsilon}{\underline{\varepsilon}} \quad (1)$$

where S_i is the ith spectrum region (referring to Figure 6 and 7) of the N regions representing the contribution investigated, $\underline{\varepsilon} = \int \varepsilon f(\varepsilon) d\varepsilon$ is the mean deposited energy, and $f(\varepsilon)$ is the ε probability density function. The contributions from the whole low-energy tail and from the region of the tail where the contribution of bridges exists are reported in **Table 1**.

Table 1. Contribution to the mean deposited energy $\underline{\varepsilon}$ from the low energy deposition tail, as measured by AμDOS prototypes when irradiated by a 6 MeV carbon ions microbeam at the RBI (Zagreb, Croatia). Two cases are reported, with reference to Figure 6 and 7: when considering all the tail regions (blue, green, and orange), and when considering only those regions where the bridges contribute to the tail (blue and green).

	Whole tail [%]	Where bridges contribute [%]
10 μm diameter SVs	46.08	32.10
40 μm diameter SVs	14.43	6.71

The contribution of the low energy tail to the deposited energy spectrum is about 14% and 46% for SVs of 40 and 10 μm diameter, respectively. As expected, the contributions are significantly lower when the SVs' area is larger. In addition, the impact of the sensitive area on the border effect is milder than its impact on the bridge effect. This could be observed in Table 1. A different proportionality between the 10 and the 40 μm SVs was found for the contribution in the case the whole low energy deposition tail is considered (larger contribution from the border), and in the case only the part of the tail where the bridges contribute is taken into account.

The bridge effect is the consequence of an undesired Schottky junction between metallic bridges and intrinsic diamond, creating an electric field beneath the bridges. Its presence generates a charge collection outside of the nominal SVs (boron-doped diamond/intrinsic diamond/Cr). Indeed, as the bias voltage is applied through the metallic electrode, the bridges are also held at the applied voltage potential. As no boron-doped diamond back-contact was grown below the metallic bridges, no p+ diamond/intrinsic diamond/metal Schottky junction was created in the bridges region. Nevertheless, a weak electric field was generated anyway if the applied potential was strong enough. The bridge effect is therefore expected to depend upon the applied voltage. The IBIC maps collected applying different bias voltage to the same irradiation conditions are shown in **Figure 8**. The behavior of the AμDOS supported the hypothesis on the origin of the bridge effect presented above.

To get rid of the bridge effect, the electronic coupling between metallic electrode and the intrinsic diamond must be avoided.

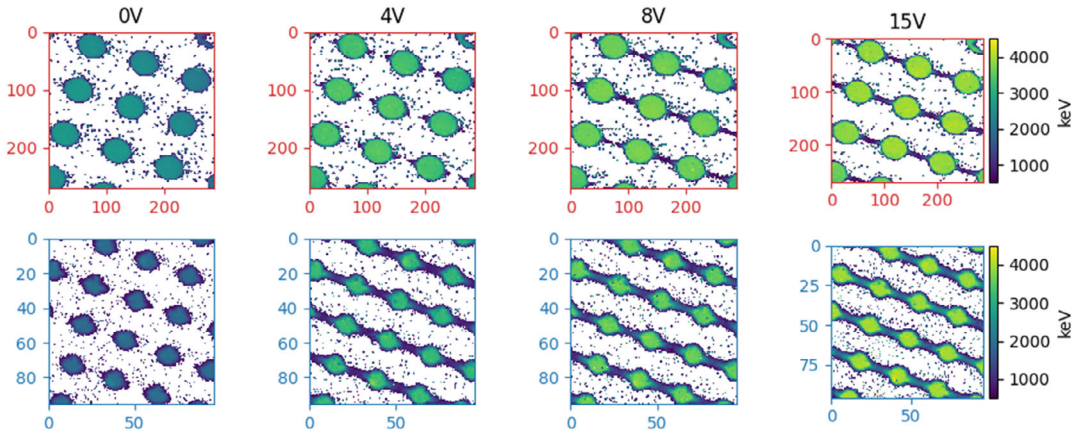

Figure 8. IBIC maps of the 40 μm diameter AμDOS prototype (red top row) and of the 10 μm diameter AμDOS prototype (blue bottom row) collected at different applied voltage as indicated above. The measurement was collected at the RBI (Zagreb, Croatia) using a 6 MeV carbon ions microbeam.

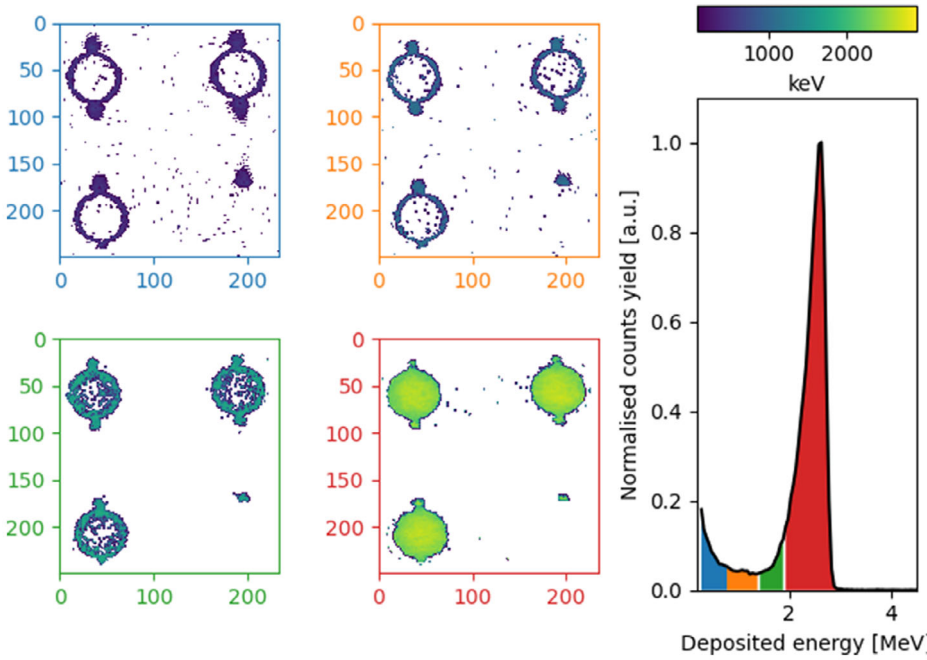

Figure 9. (Right) Deposited energy spectrum measured by the AμDOS-SG prototype when irradiated by a 6 MeV carbon ions microbeam at the Surrey Ion Beam Centre (Guildford, UK); the spectrum is divided in four regions, each one represented by a different color. (Left) The IBIC maps corresponding to each region, created by considering only events whose energy deposition occurred within the region considered; the color of the maps contour is the same color as the corresponding region.

As described in Section 2.2, two technological solutions were implemented: the AμDOS-SG and the AμDOS-IL. **Figure 9** and **10** show the results obtained when the two prototypes were irradiated by a 6 MeV carbon ions microbeam at the Surrey Ion Beam Centre. The results of the IBIC characterization were extremely promising.

Both approaches were able to neatly eliminate the generation of measurable signals from the metallic bridges, as it could be observed in Figure 9 and 10.

The bridges, indeed, were deposited either on the low-quality diamond substrate or on the insulating material in which charge carriers mobility is too low to allow them to work as radiation detectors. In Figure 9, the first few μm of bridges surrounding the SVs of the AμDOS-SG could still be observed. These regions correspond to the parts of the bridges deposited on the intrinsic diamond volume, which was grown slightly larger than the electrode size. Hence, the phenomenon observed was not the bridge effect, but it was a distortion of the SV shape, nominally circular. For a better understanding, the reader should carefully refer to Figure 9. While in Figure 6 and 7 the bridge effects clearly began at lower CCE creating the peak-like structure discussed, in Figure 9 the partial-bridge shapes could be observed in all maps

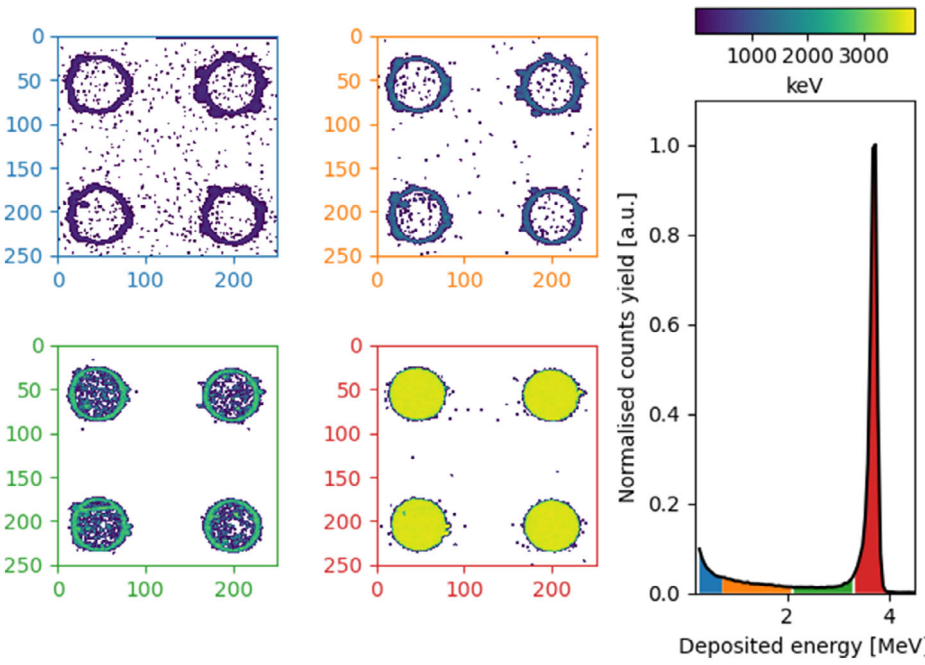

Figure 10. (Right) Deposited energy spectrum measured by the AμDOS-IL prototype when irradiated by a 6 MeV carbon ions microbeam at the Surrey Ion Beam Centre (Guildford, UK); the spectrum is divided in four regions, each one represented by a different color. (Left) The IBIC maps corresponding to each region, created by considering only events whose energy deposition occurred within the region considered; the color of the maps contour is the same color as the corresponding region.

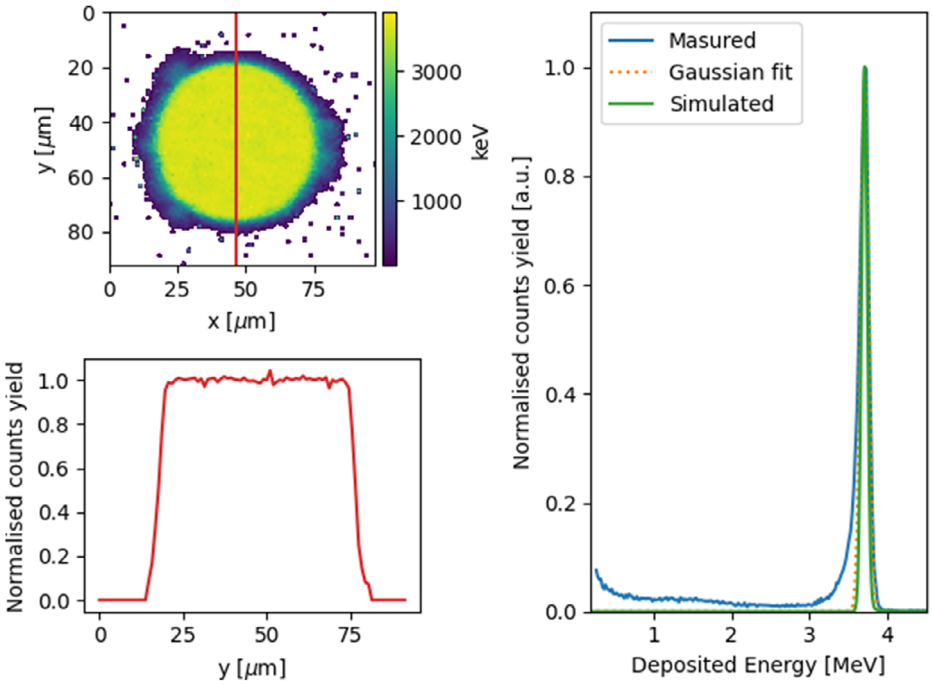

Figure 11. (Top-left) IBIC map of one of the SVs of the AμDOS-IL prototype. (Bottom-left) CCE profile of the same SV at $x = 46.5$ μm; a red line visually locates the profile on the IBIC map. (Right) The deposited energy spectrum measured by the AμDOS-IL prototype when irradiated by a 6 MeV carbon ions microbeam at the Surrey Ion Beam Centre (Guildford, UK); the Gaussian fit through which the response homogeneity was estimated, and a simulation carried out by means of SRIM are also represented.

corresponding to the four regions in the spectrum. In particular, they were found in the red region corresponding to the main peak (maximum CCE), thus showing the same behavior as the nominal SV. Hence, while major manifestations of the bridge effect were eliminated by the AμDOS-SG, such residual minor effects are still under investigation. For instance, they could be minimized by optimizing the detector layout. The results of the characterization, however, showed a criticality of the AμDOS-SG manufacturing technique. The bridge electrode is deposited all along the surface step generated by the selective growth of the intrinsic diamond only around the SVs. The steps create weak points on which the bridge electrode could break, interrupting the connection of some of the array SVs. This is what happened to the SV in the bottom right corner of the maps in Figure 9.

Figure 11 shows the IBIC map and profile of one of the 50 μm diameter SVs of the AμDOS-IL prototype, as well as the corresponding energy deposition spectrum.

As shown in Figure 11, the AμDOS-IL prototype also showed an excellent homogeneity of the response throughout the sensitive area, with a spectrum FWHM of about 3%. The SVs definition was characterized by a CCE drop from 90% to 10% of about 3.5 μm, thus resulting 1 μm worse than in the first prototype. This might be caused by the slope of the resist walls created around the etched regions (see Figure 3). Despite its isolation properties, few charges were still able to cross the thinnest region of the resist slope around the SV, generating a small collection of charge by the Cr contact. Even though the degradation of SV definition observed was small (a border region with incomplete CCE of 3.5 μm width against the 2.5 μm of the other prototypes), as the SV definition affects the measurement accuracy, future improvements of this technology will aim to minimize this effect. A sharper etching of the resist or a more precise deposition of Cr contact using dedicated masks could help improving the SV definition. Finally, for what concerns the bridge effect, the AμDOS-IL prototype achieved the complete elimination of the phenomenon, as it could be observed in Figure 10. Even if the peak-like structure could not be observed anymore in the spectrum, four energy regions were still defined to try to spot any possible contribution from the bridge. However, none of the resulting IBIC maps showed any contribution from the bridges.

The result achieved by both the AμDOS-SG and AμDOS-IL prototypes in successfully eliminating the bridge effect is highly significant. To the authors' knowledge indeed, none of the diamond AμDOSs presented in the literature have been able to perform without being affected by the bridge effect. The elimination of the bridge effect positively reflects to the microdosimeter performances, improving the measurement accuracy as it reduces the contribution from the low energy tail.

4. Summary and Conclusions

Novel layouts of diamond-based microdosimeters were developed by University of Roma "Tor Vergata." The devices consist of an array of cylindrical Schottky diodes, in which thickness and diameter could be customized. A boron-doped diamond layer was selectively grown on a low-cost diamond substrate connecting the SVs along a direction x. A Cr electrode defined the SVs, connecting them along a direction y perpendicular to the boron-doped diamond connections. This way, the boron-doped/intrinsic diamond/Cr Schottky junction (hence the charge collection region) was created only on the nominal SVs. Each SV was connected in parallel, but the proposed technologies enable reading the response of each SV separately.

Two first prototypes were manufactured with a thickness of about 1.6 μm and SVs diameter of 10 and 40 μm, respectively. The response of the two arrays and their performance were characterized by means of IBIC technique at the microbeam facility of the RBI (Zagreb, Croatia), with 6 MeV carbon ions. Both prototypes showed a good homogeneity of the response within the SVs of about 5% FWHM. A good definition of the SVs was also found, with the CCE falling from the 90% to the 10% within ≈2.5 μm. However, an undesired charge collection was observed from beneath the metallic bridges. This phenomenon, called bridge effect, is well known to affect AμDOSs and it compromises the overall SV definition and the energy deposition spectrum collected by the detector.

Two strategies were successfully implemented to improve the first version of diamond array prototypes and to get rid of the bridge effect. The first strategy was the selective growth of the intrinsic diamond layer only where the SVs will be created by the chromium electrodes. Hence, the metallic bridges are deposited on the low-quality diamond substrate, which lacks the intrinsic layer to avoid charge collection. The second strategy consisted in depositing a relatively thick insulation layer under the metallic bridges. This allowed to electrically separate metal and intrinsic diamond. A prototype was manufactured for each improvement strategy: the AμDOS-SG following the selective growth of the intrinsic solution and the AμDOS-IL following the deposition of insulation layer solution. The AμDOS-SG and the AμDOS-IL were fabricated with a diameter of 50 μm and a thickness of about 1 and 1.5 μm, respectively. The two prototypes were characterized by means of IBIC technique at the Surrey Ion Beam Centre (Guildford, UK) employing 6 MeV carbon ions. The results obtained were excellent. Both prototypes successfully eliminated the bridge effect, showing a neat definition of the SVs. The AμDOS-IL also demonstrated a good confinement of the CCE within the SVs area and a homogeneity of the response of about 3% FWHM. The AμDOS, however, showed a slightly compromised SVs shape and a weak point in the manufacturing process related to the deposition of the electrode path along the steep edges of the selectively grown intrinsic diamond volumes. Thus, the AμDOS-SG requires further improvements to be addressed in future developments of this technology.

Thanks to its simpler and more effective manufacturing process and to its better overall performance, the AμDOS-IL stood out as the best prototype in view of further developments. These will bring the proposed technology to a larger scale production and use in microdosimetry applications. Future research will focus on two aspects. On one hand, the AμDOS-IL performances will be further improved by trying to refine the SV definition by reducing the borders effect. This is currently the main limitation of the technology as it impacts the accuracy of the microdosimetric measurements. The integration of a dedicated read-out system allowing to independently read each of the array SVs will be also investigated. On the other hand, a AμDOS-IL device made of a higher number of SVs will be manufactured and used under

clinical proton and carbon beams. This will be fundamental to assess its performances in clinical beam conditions. Besides, it will allow to study and characterize the radiation quality at clinical fluence rate with higher lateral spatial resolution than what has been done so far with other diamond microdosimeters.

The developments outlined in the manuscript represent a significant advancement in the field of microdosimetry, both in terms of detector performance and practical applications. By fabricating diamond-based microdosimeter arrays with enhanced spatial resolution and CCE, this research opens up new avenues for precise and accurate measurement of radiation dose distributions at the cellular level. The versatility of the array configuration allows for tailored measurements under various fluence rate conditions, crucial for optimizing treatment protocols in particle therapy. The use of diamond, besides improving the radiation hardness with respect to silicon, provides a fairly tissue-equivalent detector increasing the suitability to radiobiological applications while maintaining the advantages of solid-state detectors. Additionally, the successful mitigation of technical challenges, such as the "bridge effect," enhances the reliability and accuracy of microdosimetric measurements, further bolstering their utility in radiobiological research and clinical practice.

Overall, these advancements pave the way for improved radiation dosimetry techniques, ultimately leading to better understanding and management of radiation effects in various applications, including cancer treatment and radiation protection.

Acknowledgements

The experiment performed at Ruder Boškovic Institute's Laboratory for Ion Beam Interactions was supported by the RADIATE project (Horizon2020) 21002532-ST "IBIC characterization of single crystal diamond devices for microdosimetry application." The experimental time at Surrey Ion Beam Centre was funded by EPSRC industrial CASE award. The authors thank all staff of the ion beam facility of Ruđer Boskovic Institute in Zagreb (Croatia) and of the Surrey Ion Beam Centre in Guildford (UK) for their precious technical support.

Conflict of Interest

The authors declare no conflict of interest.

Data Availability Statement

The data that support the findings of this study are available from the corresponding author upon reasonable request.

Keywords

array detectors, diamond detectors, ion beam-induced charge collection, microdosimetry, particle therapy

Received: December 29, 2023
Revised: April 25, 2024
Published online: June 7, 2024

[1] H. H. Rossi, M. Zaider, *Microdosimetry and its Applications*, Springer, Berlin, Heidelberg **1996**.
[2] G. Magrin, H. Palmans, M. Stock, D. Georg, *Radiother. Oncol.* **2023**, *182*, 109586.
[3] G. Parisi, F. Romano, G. Schettino, *Front. Phys.* **2022**, *10*, 1035956.
[4] P. Colautti, G. Magrin, H. Palmans, M. A. Cortés-Giraldo, V. Conte, *Front. Phys.* **2020**, *8*, 550458.
[5] P. Kliauga, A. J. Waker, J. Barthe, *Radiat. Prot. Dosim.* **1995**, *61*, 309.
[6] J. Booz, L. Braby, J. Coyne, P. Kliauga, L. Lindborg, H.-G. Menzel, N. Parmentier, *J. ICRU* **1983**, *os19*, https://doi.org/10.1093/jicru/os19.1.Report36.
[7] S. Gerdung, P. Pihet, J. E. Grindborg, H. Roos, U. J. Schrewe, H. Schuhmacher, *Radiat. Prot. Dosim.* **1995**, *61*, 381.
[8] Y. Kase, W. Yamashita, N. Matsufuji, K. Takada, T. Sakae, Y. Furusawa, H. Yamashita, S. Murayama, *J. Radiat. Res.* **2013**, *54*, 485.
[9] A. Bianchi, A. Selva, M. Rossignoli, F. Pasquato, M. Missiaggia, E. Scifoni, C. La Tessa, F. Tommasino, V. Conte, *Radiat. Phys. Chem.* **2023**, *202*, 110567.
[10] V. Conte, A. Bianchi, A. Selva, G. Petringa, G. A. P. Cirrone, A. Parisi, F. Vanhavere, P. Colautti, *Phys. Med.* **2019**, *64*, 114.
[11] S. Hartzell, F. Guan, P. Taylor, C. Peterson, P. Taddei, S. Kry, *Phys. Med. Biol.* **2021**, *66*, 155018.
[12] P. D. Bradley, A. B. Rosenfeld, M. Zaider, *Nucl. Instrum. Methods Phys. Res., Sect. B* **2001**, *184*, 135.
[13] G. Magrin, S. Barna, C. Meouchi, A. Rosenfeld, H. Palmans, *J. Nucl. Eng.* **2022**, *3*, 128.
[14] S. Agosteo, P. G. Fallica, A. Fazzi, M. V. Introini, A. Pola, G. Valvo, *Radiat. Meas.* **2008**, *43*, 585.
[15] A. B. Rosenfeld, *Nucl. Instrum. Methods Phys. Res., Sect. A* **2016**, *809*, 156.
[16] L. T. Tran, D. Bolst, B. James, V. Pan, J. Vohradsky, S. Peracchi, L. Chartier, E. Debrot, S. Guatelli, M. Petasecca, M. Lerch, D. Prokopovich, Ž. Pastuović, M. Povoli, A. Kok, T. Inaniwa, S. H. Lee, N. Matsufuji, A. B. Rosenfeld, *Appl. Sci.* **2022**, *12*, 328.
[17] C. Guardiola, D. Bachiller-Perea, J. Prieto-Pena, M. C. Jiménez-Ramos, J. García López, C. Esnault, C. Fleta, D. Quirion, F. Gómez, *Phys. Med. Biol.* **2021**, *66*, 114001.
[18] D. Bachiller-Perea, M. Zhang, C. Fleta, D. Quirion, D. Bassignana, F. Gómez, C. Guardiola, *Front. Phys.* **2022**, *10*, 958648.
[19] K. Haenen, M. Nesladek, *Phys. Status Solidi A* **2013**, *210*, 1960.
[20] J. A. Davis, P. Lazarakis, J. Vohradsky, M. L. F. Lerch, M. Petasecca, S. Guatelli, A. B. Rosenfeld, *Radiat. Meas.* **2019**, *122*, 1.
[21] J. A. Davis, K. Ganesan, A. D. C. Alves, S. Guatelli, M. Petasecca, J. Livingstone, M. L. F. Lerch, D. A. Prokopovich, M. I. Reinhard, R. N. Siegele, S. Prawer, D. Jamieson, Z. Kuncic, V. L. Pisacane, J. F. Dicello, J. Ziegler, M. Zaider, A. B. Rosenfeld, *IEEE Trans. Nucl. Sci.* **2012**, *59*, 3110.
[22] J. A. Davis, M. Petasecca, S. Guatelli, M. L. F. Lerch, A. B. Rosenfeld, *J. Phys.: Conf. Ser.* **2019**, *1154*, 012007.
[23] I. A. Zahradnik, M. T. Pomorski, L. De Marzi, D. Tromson, P. Barberet, N. Skukan, P. Bergonzo, G. Devès, J. Herault, W. Kada, T. Pourcher, S. Saada, *Phys. Status Solidi A* **2018**, *215*, 1800383.
[24] I. A. Zahradnik, P. Barberet, D. Tromson, L. De Marzi, M. T. Pomorski, *Rev. Sci. Instrum.* **2020**, *91*, 54102.
[25] C. Verona, G. Magrin, P. Solevi, M. Bandorf, M. Marinelli, M. Stock, G. Verona Rinati, *Radiat. Meas.* **2018**, *110*, 25.
[26] C. Verona, G. Magrin, P. Solevi, V. Grilj, M. Jakšić, R. Mayer, M. Marinelli, G. Verona-Rinati, *J. Appl. Phys.* **2015**, *118*, 184503.

[27] M. Jakšić, I. Bogdanović Radović, M. Bogovac, V. Desnica, S. Fazinić, M. Karlušić, Z. Medunić, H. Muto, Ž. Pastuović, Z. Siketić, N. Skukan, T. Tadić, *Nucl. Instrum. Methods Phys. Res., Sect. B* **2007**, *260*, 114.
[28] P. J. Sellin, A. Lohstroh, A. Simon, M. B. H. Breese, *Nucl. Instrum. Methods Phys. Res., Sect. A* **2004**, *521*, 600.
[29] A. Simon, C. Jeynes, R. P. Webb, R. Finnis, Z. Tabatabaian, P. J. Sellin, M. B. H. Breese, D. F. Fellows, R. Van Den Broek, R. M. Gwilliam, *Nucl. Instrum. Methods Phys. Res., Sect. B* **2004**, *219–220*, 405.
[30] J. F. Ziegler, M. D. Ziegler, J. P. Biersack, *Nucl. Instrum. Methods Phys. Res., Sect. B* **2010**, *268*, 1818.
[31] D. Bachiller-Perea, J. G. Lopez, M. C. Jimenez-Ramos, F. Gomez, C. Fleta, D. Quirion, A. Garcia-Osuna, C. Guardiola, *IEEE Trans. Instrum. Meas.* **2021**, *70*, 6005211.
[32] L. T. Tran, L. Chartier, D. A. Prokopovich, M. I. Reinhard, M. Petasecca, S. Guatelli, M. L. F. Lerch, V. L. Perevertaylo, M. Zaider, N. Matsufuji, M. Jackson, M. Nancarrow, A. B. Rosenfeld, *IEEE Trans. Nucl. Sci.* **2015**, *62*, 504.
[33] L. T. Tran, L. Chartier, D. A. Prokopovich, D. Bolst, M. Povoli, A. Summanwar, A. Kok, A. Pogossov, M. Petasecca, S. Guatelli, M. I. Reinhard, M. Lerch, M. Nancarrow, N. Matsufuji, M. Jackson, A. B. Rosenfeld, *IEEE Trans. Nucl. Sci.* **2018**, *65*, 467.